

# Journal of Visualized Experiments

## Three and four-dimensional visualization and analysis approaches to study vertebrate axial elongation and segmentation --Manuscript Draft--

Article Type:	Invited Methods Article - JoVE Produced Video
Manuscript Number:	JoVE62086R2
Full Title:	Three and four-dimensional visualization and analysis approaches to study vertebrate axial elongation and segmentation
Corresponding Author:	Moisés Mallo Instituto Gulbenkian de Ciencia Oerias, PORTUGAL
Corresponding Author's Institution:	Instituto Gulbenkian de Ciencia
Corresponding Author E-Mail:	mallo@igc.gulbenkian.pt
Order of Authors:	André Dias Gabriel Martins Alexandre Lopes Moisés Mallo
Additional Information:	
Question	Response
Please specify the section of the submitted manuscript.	Developmental Biology
Please indicate whether this article will be Standard Access or Open Access.	Standard Access (US\$2,400)
Please indicate the <b>city, state/province, and country</b> where this article will be <b>filmed</b> . Please do not use abbreviations.	Lisbon/Portugal
Please confirm that you have read and agree to the terms and conditions of the author license agreement that applies below:	I agree to the <a href="#">Author License Agreement</a>
Please provide any comments to the journal here.	

**TITLE:**

Three and four-dimensional visualization and analysis approaches to study vertebrate axial elongation and segmentation

**AUTHORS AND AFFILIATIONS:**

André Dias<sup>1#</sup>, Gabriel G. Martins<sup>1#</sup>, Alexandre Lopes<sup>1</sup>, Moisés Mallo<sup>1#</sup>

# - corresponding authors

1. Instituto Gulbenkian de Ciência, Oeiras, Portugal
2. Faculdade de Ciências da Universidade de Lisboa, Lisbon, Portugal
3. NOVA School of Science and Technology, Lisbon, Portugal

AD: [amdias@igc.gulbenkian.pt](mailto:amdias@igc.gulbenkian.pt)

GG: [gaby@igc.gulbenkian.pt](mailto:gaby@igc.gulbenkian.pt)

AL: [alopes@igc.gulbenkian.pt](mailto:alopes@igc.gulbenkian.pt)

MM: [mallo@igc.gulbenkian.pt](mailto:mallo@igc.gulbenkian.pt)

**KEYWORDS:**

3D reconstruction; live imaging; vertebrate; mouse embryonic development; somitogenesis; mesoderm; axial extension; NMPs; immunofluorescence; clearing techniques; imaging analysis; teaching.

**SUMMARY:**

Here, we describe computational tools and methods that allow visualization and analysis of three and four-dimensional image data of mouse embryos in the context of axial elongation and segmentation, obtained by in toto optical projection tomography, and by live imaging and whole-mount immunofluorescence staining using multiphoton microscopy.

**ABSTRACT:**

Somitogenesis is a hallmark of vertebrate embryonic development. For years, researchers have been studying this process in a variety of organisms using a wide range of techniques encompassing ex vivo and in vitro approaches. However, most studies still rely on the analysis of two-dimensional (2D) imaging data, which limits proper evaluation of a developmental process like axial extension and somitogenesis involving highly dynamic interactions in a complex 3D space. Here we describe techniques that allow mouse live imaging acquisition, dataset processing, visualization and analysis in 3D and 4D to study the cells (e.g., neuromesodermal progenitors) involved in these developmental processes. We also provide a step-by-step protocol for optical projection tomography and whole-mount immunofluorescence microscopy in mouse embryos (from sample preparation to image acquisition) and show a pipeline that we developed to process and visualize 3D image data. We extend the use of some of these techniques and highlight specific features of different available software (e.g., Fiji/ImageJ, Drishti, Amira and Imaris) that can be used to improve our current understanding of axial extension and somite formation (e.g., 3D reconstructions). Altogether, the techniques here described emphasize the importance of 3D data visualization and analysis in developmental biology, and might help other researchers to better address 3D

and 4D image data in the context of vertebrate axial extension and segmentation. Finally, the work also employs novel tools to facilitate teaching vertebrate embryonic development.

## INTRODUCTION:

Vertebrate body axis formation is a highly complex and dynamic process occurring during embryonic development. At the end of gastrulation [in the mouse, around embryonic day (E) 8.0], a group of epiblast progenitor cells known as neuromesodermal progenitors (NMPs) become a key driver of axial extension in a head to tail sequence, generating the neural tube and paraxial mesodermal tissues during neck, trunk and tail formation<sup>1-4</sup>. Interestingly, the position that these NMPs occupy in the caudal epiblast seems to play a key role in the decision of differentiating into mesoderm or neuroectoderm<sup>5</sup>. Although we currently lack a precise molecular fingerprint for NMPs, these cells are generally thought to co-express T (Brachyury) and Sox2<sup>5,6</sup>. The exact mechanisms regulating NMP fate decisions (i.e., whether they take neural or mesodermal routes) are only starting to be precisely defined. *Tbx6* expression in the primitive streak region is an early marker of NMP fate decision, as this gene is involved in the induction and specification of mesoderm<sup>6,7</sup>. Interestingly, early mesoderm cells seem to express high levels of *Epha1*<sup>8</sup>, and *Wnt/b-catenin* signalling, as well as *Msgn1* were also shown to play important roles in paraxial mesoderm differentiation and somite formation<sup>9,10</sup>. A complete spatial-temporal analysis of NMPs at a single-cell level will certainly be instrumental to fully understand the molecular mechanisms controlling mesoderm specification.

The formation of somites (vertebrae precursors) is a key feature of vertebrates. During axial elongation, the paraxial mesoderm becomes segmented in a series of bilateral repeating units known as somites<sup>11,12</sup>. The number of somites and the time required for the formation of new segments varies among species. Somitogenesis involve periodic signaling oscillations (known as the “segmentation clock”) that can be observed by the cyclic expression of several genes of the *Notch*, *Wnt* and *Fgf* signalling pathways in the presomitic mesoderm (e.g., *Lfng*)<sup>11,12</sup>. The current model of somitogenesis also postulates the existence of a “maturation wavefront”, a series of complex signalling gradients involving Fgf, Wnt and retinoic acid signaling that define the position of the posterior border of each new somite. A coordinated interaction between the “segmentation clock” and the “maturation wavefront” is therefore fundamental for the generation of these vertebrae precursor modules as perturbations in these key morphogenetic processes can result in embryonic lethality or in the formation of congenital malformations (e.g., scoliosis)<sup>13-15</sup>.

Despite substantial recent advances in imaging techniques, bioimage analysis methods and software, most studies of axial elongation and somitogenesis still rely on single/isolated two-dimensional image data (e.g., sections), which does not allow a full multidimensional tissue visualization and complicates clear differentiation between pathological malformations (i.e., due to mutations) vs normal morphological variation occurring during embryonic development<sup>16</sup>. Imaging in 3D has already uncovered novel morphogenetic movements, previously not identified by standard 2D methods<sup>17-20</sup>, highlighting the power of in toto imaging to understand the mechanisms of vertebrate somitogenesis and axial extension.

3D and 4D microscopy of mouse embryos, particularly live imaging, are technically challenging and require critical steps during sample preparation, image acquisition and data pre-processing in order to allow an accurate and meaningful spatio-temporal analysis. Here, we

describe a detailed protocol for live imaging and whole-mount immunofluorescence staining of mouse embryos, that can be used to study both NMPs and mesodermal cells during axial extension and segmentation. In addition, we also describe a protocol for optical projection tomography (OPT) of older embryos and fetuses, that allows 3D in toto visualization and quantification of pathological abnormalities that can result from problems during somitogenesis (e.g., bone fusion and scoliosis)<sup>13,21,22</sup>. Finally, we illustrate the power of 3D imaging reconstructions in the study and teaching of vertebrate segmentation and axial elongation.

## PROTOCOL:

Experiments involving animals followed the Portuguese (Portaria 1005/92) and European (Directive 2010/63/EU) legislations concerning housing, husbandry, and welfare. The project was reviewed and approved by the Ethics Committee of 'Instituto Gulbenkian de Ciência' and by the Portuguese National Entity, 'Direcção Geral de Alimentação Veterinária' (license reference: 014308).

### 1. Sample preparation for 3D and 4D imaging

NOTE: Here we provide a detailed description on how to dissect and prepare mouse E8.25 to E10.5 embryos for live imaging (1.1), E7.5 to E11.5 embryos for whole mount immunofluorescence microscopy (1.2) and fetuses for optical projection tomography (1.3).

#### 1.1. Sample preparation for live imaging

##### 1.1.1. Mouse embryo dissection and preparation for live imaging (e.g., LuVeLu reporter<sup>23</sup>).

1.1.1.1. Dissect mouse embryos between E8.25 and E10.5 in pre-warmed M2 medium (37 °C). Gently remove the yolk sac using clean forceps and wash the embryo once with fresh M2 medium to remove blood and debris produced during dissection.

NOTE: It is important to avoid damaging the embryo in any way, otherwise it will not develop properly during the live imaging procedure.

1.1.1.2. During the live imaging procedure, incubate embryos in a heated chamber (37 °C), in a 65% O<sub>2</sub> and 5% CO<sub>2</sub> environment (N<sub>2</sub> balanced), in low glucose DMEM medium supplemented with 10% HyClone defined fetal bovine serum, 2 mM L-glutamine and 1% penicillin-streptomycin.

NOTE: These culture conditions allow embryonic development to occur for around 10 h. Other protocols<sup>9,10</sup>, using different culture conditions, might allow even longer periods.

#### 1.2. Sample preparation for immunofluorescence microscopy

##### 1.2.1 Mouse embryo dissection and fixation procedure



1.2.1.1. Dissect mouse embryos from E7.5 to E11.5 in either cold (4 °C) phosphate buffered saline (PBS) or M2 medium. After removal of all extra-embryonic membranes (e.g., Reichart's membrane or yolk sac) wash the embryo in fresh PBS to remove blood and debris produced during the dissection procedure.

1.2.1.2. Fix embryos at 4 °C, in 4% paraformaldehyde (PFA) in PBS, for the time specified in **Table 1**.

CAUTION – PFA should be handled inside a fume hood.

[place Table 1 here]

1.2.1.3. After fixation, wash embryos at least twice (5-10 min each) in PBS to remove PFA completely. At this point, embryos can be taken straight into the immunofluorescence staining protocol (Step 1.2.2) or can be dehydrated and stored for future use (Step 1.2.1.4).

1.2.1.4. If needed, store embryos at -20 °C in 100% methanol for long periods.

1.2.1.4.1. To improve tissue preservation, dehydrate the embryo dehydration gradually with 10% increases in methanol concentration (diluted in PBS), each step 10 min at room temperature (RT) on a shaker, until reaching 100% methanol. Replace the 100% methanol once using a fresh aliquot.

1.2.1.4.2. Recover frozen embryos by rehydration following a reverse methanol/PBS series, each step 10 min at RT on a shaker, and with final washes in PBS (twice, 5-10 min each) before entering the immunostaining protocol.

CAUTION - Methanol should be handled inside a fume hood.

## 1.2.2. Whole-mount immunofluorescence staining

NOTE: The following immunofluorescence staining protocol was adapted from the procedure described in Osorno et al.<sup>24</sup>. All washes should be performed on a shaker. After the blocking step, incubations are performed at 4 °C to ensure antibody integrity/preservation.

1.2.2.1. Wash embryos three times (30 min each) in PBS containing 0.1% Triton X-100 (0.1% PBST) and then once in 0.5% PBST for 1 hour (RT) to improve permeabilization.

1.2.2.2. To reduce nonspecific binding, wash in 1 M of glycine in PBS (pH 7.5) for 30 min at RT.

1.2.2.3. Wash three times in 0.1% PBST for 30 min to completely remove the glycine.

1.2.2.4. Incubate the embryos, overnight at 4 °C, in blocking solution containing: 3% of serum (from the animal species in which the secondary antibodies were produced), 1% of bovine serum albumin (BSA) and 0.1% of Triton X-100, in PBS.

1.2.2.5. Dilute primary antibodies in blocking solution (normally 1:200 for T and Sox2 antibodies) and incubate for two to three days at 4 °C.

1.2.2.6. Before adding the secondary antibodies, wash embryos three times (30 min each) in 0.1% PBST at 4 °C. Dilute secondary antibodies in blocking solution (1:1000) and incubate for 2 days at 4 °C, protected from light.

1.2.2.7. Wash embryos six times (30 min each) in 0.1% PBST at 4 °C.

1.2.2.8. For nuclear counterstaining, incubate embryos in 4',6-Diamidino-2-Phenylindole, Dihydrochloride (DAPI), diluted 1:500 in PBST, overnight on a shaker at 4 °C, protected from light.

1.2.2.9. Finally, wash embryos three times (30 min each) in 0.1% PBST at 4 °C.

### 1.2.3. Tissue clearing and slide preparation

#### 1.2.3.1. Tissue clearing using methyl salicylate or a mixture of benzyl alcohol with benzyl benzoate (BABB)

1.2.3.1.1. Before clearing using methyl salicylate or BABB, completely dehydrate embryos by bringing them to 100% methanol, through a methanol/PBS series at 4 °C, consisting of successive 10% increases in methanol concentration (incubation times of 10 min each). To achieve complete dehydration, replace the 100% methanol for a fresh one and wait for an additional 10 min.

1.2.3.1.2. Perform embryo clearing by embedding in a series of methyl salicylate or BABB in methanol with 20% successive increases in concentration, 20 minute incubation for each step. When the methyl salicylate or BABB solution reaches 100% make two additional changes for a fresh solution.

CAUTION: Both methyl salicylate and BABB should be handled inside a fume hood.

NOTE: For proper clearing, it is essential that embryos are fully dehydrated. It is also essential that the methanol is fully mixed with methyl salicylate or BABB in the clearing solution series.

1.2.3.1.3. After the embryos become completely transparent, handle them individually, using preferentially a fluorescence stereoscope, to reduce the chances of tissue damage.

1.2.3.1.4. For imaging, mount embryos in either a 75 mm x 25 mm depression concave glass slide or a 20 mm x 60 mm #1.5 coverglass. The latter option will allow imaging from both sides, if necessary, but it is much more fragile and difficult to seal. Transfer embryos to the microscope slides using a toothpick, a fine cotton tip, a Pasteur pipette or any other similar instrument.

1.2.3.1.5. To avoid compressing the embryos, add spacers made from #1 coverglass shards (170  $\mu$ m thick), silicone or thin metal washers. Then add a drop of mounting medium, cover with a #1 or #0 20x20 mm coverglass and seal.

1.2.3.1.6. If using glass or metal spacers, seal with melted paraffin to better stabilize the preparation - do not seal with nail-polish because it dissolves with methyl salicylate or BABB. To avoid bubbles, place the coverslip on one side and then, gradually and gently slide it sideways; add more medium if necessary.

NOTE: Please see the video to better understand how to manipulate the cleared embryos and how to mount them on the microscope slide.

### 1.2.3.2. Tissue clearing

1.2.3.2.1. When using the clearing solution (e.g., RapiClear), embryo dehydration is not required. After Step 1.2.2.9, place embryos in the center of a 75 mm x 25 mm depression concave glass slide, remove all the PBST in the microscope depression slide and add 200  $\mu$ L of clearing solution.

1.2.3.2.2. After 10 min protected from light, when embryos start to become transparent, replace the clearing solution, wait an additional 20 min (protected from light) and then top with a coverslip, starting from one side and gently moving towards the other.

NOTE: The time to fully clear the embryo may go from a few minutes to overnight depending on the stage and size of embryos. Also, the entire process should be done under a stereomicroscope. To better understand the clearing and the microscope slide preparation, please see the video protocol.

## 1.3. Sample preparation for optical projection tomography

NOTE: The following procedures were adapted from previous protocols<sup>19,25,26</sup>. The protocol will be described for the analysis of E18.5 mouse fetuses.

### 1.3.1. Mouse fetus dissection and fixation procedure

1.3.1.1. Dissect E18.5 mouse fetuses in cold (4 °C) PBS, remove all extra-embryonic membranes and then wash the fetuses several times in fresh PBS to remove blood and debris produced during the dissection procedure.

1.3.1.2. Fix fetuses in 4% PFA made in PBS, at 4 °C for 5 to 7 days.

1.3.1.3. Wash fetuses once (15 min) in PBS and then three times (30 min each) in demineralized water or PBS. Perform the washes on a shaker.

1.3.1.4. Dehydrate the fetuses by incubation (25 min series at RT on a shaker) in methanol solutions of increasing concentrations (10% increases diluted in demineralized water or PBS) until 100% methanol.

1.3.1.5. Change the 100% methanol solution (use a fresh aliquot) three times (20 min each) to ensure complete dehydration. Embryos can then be stored at -20 °C or be taken directly (one day later) to the bleaching process (Step 1.3.2).

### 1.3.2. Bleaching process

1.3.2.1. To remove the natural pigmentation, incubate fetuses (separately) on a shaker, first for one day in 5% demineralized water (or PBS) in methanol and then in 10% demineralized water (or PBS) in methanol for up to 3 days until the embryos lose all the natural pigmentation.

CAUTION: H<sub>2</sub>O<sub>2</sub> should be handled gently inside a fume hood. The bleaching solution containing H<sub>2</sub>O<sub>2</sub> when in contact with the specimen creates vapors and, therefore, the tube containing the fetuses should remain open during the entire bleaching procedure. Some bleaching protocols suggest the combination of H<sub>2</sub>O<sub>2</sub> with formamide. If this alternative is used, extra-care must be taken, as adding H<sub>2</sub>O<sub>2</sub> to undiluted formamide can result in an explosion.

1.3.2.2. Gradually rehydrate the embryos in a reverse methanol series (with 10% decrease) in demineralized water, each incubated for 20 min at RT on a shaker, and finally wash three times (30 min each) in demineralized water. Wait one day, change the demineralized water and proceed further.

NOTE: See **Supplemental Figure 1** for a representative result of the bleaching process.

### 1.3.3. Demineralization protocol

NOTE: Demineralization is optional but recommended for fetuses or pups.

1.3.3.1. Perform demineralization by washing the fetuses in 0.1 M EDTA at 42 °C for a few hours [see also Cho et al.<sup>27</sup>] followed by five washes (20 min each) with demineralized water to completely remove the EDTA. Perform all procedures on a shaker.

### 1.3.4. Sample preparation for clearing

1.3.4.1. Embed fetuses in a 1% agarose block. To prepare these blocks fill a 50 mL plastic tube or syringe (building a cylindrical space by cutting off the syringe's exit side and using the plunger to block the opposite side) with melted agarose, place the fetus in the agarose in a vertical position and keep this position at the center of the block with the aid of forceps during solidification of the agarose.

1.3.4.2. Place the mold with the block at 4 °C (30 min) for the agarose to fully jellyfy. In case of incorrect positioning of the fetus within the block or the appearance of air bubbles, melt the agarose by placing the block at 50 °C overnight, and repeat the procedure on the next day.

1.3.4.3. Remove the agarose block with the fetus from the mold and place it in a container with demineralized water. Replace with fresh demineralized water after 15 min.

1.3.4.4. Before clearing with BABB, dehydrate the specimen. To better preserve tissue integrity, perform fetus dehydration gradually with 10% increases in methanol concentration (diluted in demineralized water or PBS), each step for more than 45 min at RT on a shaker, until reaching 100% methanol.

1.3.4.5. Change the 100% methanol (use a fresh aliquot), first four times in one hour intervals and then again on the following day to ensure complete dehydration.

### 1.3.5. Clearing process and sample mounting for OPT imaging

1.3.5.1. Clear the fetuses on a shaker through a series (2.5 hours each) of BABB solution in methanol, with 25% increases in BABB concentration, until reaching 100% BABB.

1.3.5.2. Replace the BABB solution with a fresh one every day, until the fetus is completely transparent. This process might take 3 to 5 days. Keep the block containing the fetus, on a shaker during the entire procedure. Fetuses can stay in 100% BABB solution for long periods.

NOTE: If the fetus is not correctly dehydrated it will become slightly translucent (“whitish” emulsion) after first adding BABB. If this happens, step back into pure methanol and perform two additional washes in fresh methanol. Never refrigerate samples while performing dehydration and clearing, as the changes in temperature may lead to water condensation.

1.3.5.3. Attach the cleared agarose block to the motor axis of the OPT scanner, adjust optics to obtain an image of the whole fetus and proceed to acquiring a full projection dataset<sup>19,28</sup>.

## 2. Microscope/Image acquisition

2.1. For correct 3D and 4D imaging, choose the microscope that best fits the experimental goal. **Table 2** provides general information to guide through the selection.

[Place Table 2 here]

## 3. Image dataset pre-processing

NOTE: Here we highlight some of the key steps of image dataset pre-processing, namely noise reduction (3.1) and deconvolution (3.2) and provide algorithms that allow proper preparation and pre-processing of 3D datasets time-series (3.3) and whole-mount immunofluorescence stainings (3.4). Finally, we indicate references that describe in detail a protocol for OPT dataset pre-processing and reconstruction.

### 3.1. Noise reduction

3.1.1. If the images show reduced signal-to-noise ratio, consider applying a classical method such as a “Median” filter or “Anisotropic diffusion” available in Fiji/ImageJ<sup>29</sup>, or a more elaborate method based on Machine Learning such as “CARE”<sup>30</sup> or “Noise2Void”<sup>31</sup>.

NOTE: This is especially relevant for live imaging datasets, where the photobleaching and photodamage is a major concern, and lower exposures and higher detector gains are necessary.

## 3.2. Deconvolution

3.2.1. If the images were acquired with high-resolution (near or at Nyquist sampling) consider performing image restoration with deconvolution to enhance the quality of the dataset before analysis. Beware that some deconvolution tools also include a denoising step.

NOTE: This has been extensively addressed in Krull et al.<sup>32</sup> and in documentation available at the Huygens deconvolution software website (<https://svi.nl/HomePage>).

## 3.3. Preparing a 3D dataset time-series for proper visualization and analysis

NOTE: Often embryo or stage drift can occur during time-lapse imaging. This needs to be corrected before performing analysis. Sometimes, the drift is severe enough that the acquisition needs to be interrupted and adjustments made. In this case, make sure to keep the same X, Y and Z dimensions.

3.3.1. Separate 4D stacks can be concatenated into a single 4D hyperstack using Fiji’s “concatenate” function. However, this tool does not handle composite/hyperstacks, so it is necessary to convert all 4D segments into simple stacks using the operation **Image | Hyperstacks | Hyperstack to stack**. Keep some numbering system to maintain the order of these 4D segments and take note of the information about each one (channels, slices, time-points). Repeat the procedure for all segments and then concatenate them using the procedure **Image | Stacks | Tools | Concatenate**.

3.3.2. Reconstruct the concatenated hyperstack with the operation **Image | Hyperstacks | Stack to Hyperstack** and choose the correct order of the different dimensions. Inspect the Hyperstack to make sure all dimensions are correctly sequenced.

NOTE: The number of **Channels (c)** and **Slices (z)** should be the same for all 4D segments; the number of (time) **Frames (t)** should be equal to the total of time points added for all 4D segments. It is important to browse through the stack to understand how the different dimensions are interpolated, before performing the conversion to hyperstack. Fiji/ImageJ default is alternating channels, then alternating Z slices, and then alternating time-points (“XYCZT”). Confirm that this applies to the data generated by the microscope.

3.3.3. Choose **Composite** as the **Display mode** and save as Tagged Image File Format (TIFF). For large datasets, consider converting to BigDataViewer<sup>33</sup> format, by performing the operation **Plugins | BigDataViewer | Export Current Image as XML/HDF5**. This generates a

dataset that can be browsed more efficiently and in 3D using the BigDataViewer and can be handled by other Fiji/ImageJ tools for big-data datasets.

3.3.4. Register the concatenated hyperstack (time-series of 3D stacks) to compensate for embryo/stage drift using either the “Correct 3D Drift” ImageJ plugin<sup>34</sup> or the BigStitcher plugin<sup>35</sup>, depending on the degree of the drift correction needed. XML/HDF5 files can be opened with BigStitcher.

NOTE: It is necessary to perform the registration of 3D time-lapses that show embryo drift before any attempt to perform cell tracking or movement analysis; correcting for drift is also necessary to properly interpret morphogenetic movements.

### 3.4. Pre-processing of datasets of immunofluorescence imaging

#### 3.4.1. Z-depth signal attenuation

NOTE: Although the method we propose to correct signal attenuation can be useful, this should be used carefully, as often less signal in depth may actually reflect a biological and not an optical phenomenon. Consider measuring the decay in an area of tissue where the molecule of interest is not expected to be present or expressed and adjust the compensation for that area. If there is still a lower positive signal in depth, it may reveal an actual biological phenomenon. Consider also that some areas of the sample may produce more scattering or laser attenuation than others, and that it will not be fully corrected with this simple method.

3.4.1.1 For thicker/late-stage embryos, beam attenuation, photobleaching and spherical aberration caused by mismatch of refractive indices (between the mounting medium and the microscope objective), can result in datasets where the fluorescence intensity is greatly attenuated in the deeper slices of the Z-stack. Therefore, compensate for this loss of signal before analysis. Determining analytically the most accurate attenuation is complex and highly sample dependent<sup>36</sup>, but a quick approximation can be determined empirically in ImageJ/Fiji using the **Process | Math | Macro** function and clicking on **Preview**.

3.4.1.2 Load the Z-stack in Fiji/ImageJ and then perform the procedure **Image | Stacks | Reslice**. Start at: **top**, keep **Avoid interpolation** ticked and **OK**. Now the “Z” will be the “Y” axis. Next, do **Image | Lookup tables (LUT) | Fire** (or any other multi-colored LUT). This will help to assess visually the best compensation during the next steps. Switch to a slice in the middle of the embryo, where the effects of attenuation in depth are clearly visible (the intensity drops from the top [superficial] to the bottom [deeper]).

3.4.1.3 Proceed to determining the correction of the vertical (“y”) intensity drop with the procedure **Process | Math | Macro**, and add the following “Code” exactly as written here:

$$v = v * A * \exp ( B * y/h )$$

In this expression, “v” is the variable for pixel intensity (which will be adjusted as a function on depth), “y” the variable for depth, and “h” for full depth, and “exp” is an exponential function; “A” should be replaced with a number between 0.5 and 1.0 (choose lower values to avoid oversaturation of the top layers of the Z-stack); B replaced with a number between 0.5 and 2.0, depending on how severe the Z-depth attenuation is - ideally it should be 1, however

in some cases less (or more) is necessary to correctly compensate the bottom layers; a higher value of B will result in more attenuation compensation. Click on **Preview** to make a first assessment. Test different values of A and B until obtaining adequate compensation from top to bottom of the image (the “Fire” LUT can be helpful for this assessment). When satisfied, apply the settings by clicking **OK**.

NOTE: This must be performed in each channel individually, because red-shifted dyes and lasers may attenuate less, and some dyes bleach faster than others. Keep in mind that this procedure might not be accurate enough to allow reliable quantification of fluorescence intensity variations in depth, although it is certainly more reliable than performing quantifications directly in the original 3D dataset that is severely affected by attenuation of signal in depth. One way to identify and control for this effect, is to compare imaging different embryos from the dorsal and ventral sides.

3.4.1.4 Restore the original geometry of the compensated Z-stack by doing **Image | Stacks | Reslice**, start at **top**, keep **Avoid interpolation** ticked, and now the “Y” must become the “Z” plane again; replace the color by performing “**Image | Lookup tables | Grays**” (or the other LUT of choice). Discard the original non-compensated z-stack and save the compensated version.

NOTE: See **Supplemental Figure 2** as a representative result of the Z-depth signal attenuation method.

### 3.4.2. Z-axis scaling correction

3.4.2.1. If imaging with an objective designed for a refractive index different to that used for mounting the embryos, perform re-scaling of the slice thickness, otherwise measurements in depth will be incorrect (potentially by 50% if using a “dry” objective on a tissue-cleared embryo). This is explained, reviewed and the different methods discussed, in <sup>37</sup> and <sup>38</sup>. Determining analytically the actual Z-axis distortion scale is complex, but an acceptable approximation can be easily determined by finding the ratio between the refractive index of the sample and the refractive index of the objective (e.g., 1.53/1.0 for a methyl salicylate-cleared embryo imaged with a dry 20 x objective, or 1.56/1.33 for an embryo cleared with BABB and imaged with a water immersion objective).

3.4.2.2. With the Z-stack dataset already opened in Fiji/ImageJ (for multichannel images, after they were assembled as “composite” with all channels), go to **Image | Properties** and change the **Voxel depth** to the slice thickness obtained during image acquisition multiplied by the Z-axis scaling correction determined in the previous step (4.2.1; “Image dataset pre-processing” section). Confirm the result using the **Image | Stacks | Orthogonal Views**.

### 3.4.3. Repositioning of embryo to an anatomically standard position using Fiji/ImageJ

NOTE: Repositioning the embryo (see the advantages highlighted in **Supplemental Figure 3**) into a standardized anterior-posterior [A-P] and dorsal-ventral [D-V] axis position using



Fiji/ImageJ, requires the installation of the TransformJ <sup>39</sup> suite of plugins from Fiji's "ImageScience" update website.

NOTE: This technique is preferable to rounds of rotations in the three planes which would introduce aliasing artifacts and degradation of resolution. However, because the Fiji/ImageJ 3D viewer plugin cannot handle properly datasets larger than 200-300 Mb (the plugin may not render or show unpredictable behavior when trying to rotate the viewing angle), the original 3D dataset must be down-sampled first.

3.4.3.1. Start by reducing the dataset size in Fiji's **Image | Scale** and then insert the X, Y and Z "scale" values necessary to reduce the dataset to less than 200 Mb (for example a 0.5 x 0.5 x 0.5 down-sampling will result in a dataset 8 times smaller). Make sure the **Create new window** option is ticked.

3.4.3.2. Then go to **Plugins | 3D viewer**. Inside the 3D viewer window, click over the embryo to select it, and a red 3D box should appear. When using this mode (with the red box activated), the rotation of the dataset can be controlled with the mouse, in contrast to the default behavior, which is to rotate the viewing angle. When repositioning the embryo with the mouse, never click outside or the dataset will be deselected.

3.4.3.3. When satisfied with the new position of the embryo, select **Edit | Transformation | Export transformed image** in the menu of the "3D viewer" window. To inspect the different orthogonal planes go to **Image | Stacks | Orthogonal Views**. If the embryo is not correctly positioned, close the window and go back to the **3D viewer** window and re-adjust. Repeat step 4.3.2 ("Image dataset pre-processing" section).

3.4.3.4. When the embryo is correctly positioned, select from the "3D viewer" window menu **Edit | Transformation | Save transform** and save the transformation matrix to a text file with the \*.mat extension. Open this text file using Fiji/ImageJ, remove the first two lines (text) and re-save. This creates a transformation matrix file compatible with the "TransformJ" plugin described in <sup>39</sup>.

3.4.3.5. Switch to the full-resolution dataset (can be a multi-channel composite hyperstack) and perform the operation **Plugins | TransformJ | TransformJ affine**. In the new window, browse to search for the matrix file previously saved, select the **Cubic B-Spline interpolation | resample isotropically | OK**.

NOTE: This operation is memory and CPU intensive. Depending on the workstation and dataset size, the operation may take from minutes to hours. The use of the "resample isotropically" option guarantees that no resolution is lost during the transformation operation, so the dataset will increase in size significantly and will no longer be anisotropic like the original confocal z-stack; it is to be expected that the number of slices in the Z-axis increases to the same number of X and Y pixels of each slice, and the stack bloated to 5-10x the original size. This is necessary to guarantee that no information is lost in the course of interpolation of voxels during rotation and translation.

3.4.3.6. Once the embryo is properly repositioned it is often possible to trim most of the empty space created around the embryo. Perform a full Z-projection **Image | Stacks | Z Project...** and choose **Maximum intensity**; draw the minimum ROI that contains the whole embryo in X and Y. Switch to the original dataset image windows, go to **Edit | Selection | Restore selection**, and crop by selecting **Image | crop**.

3.4.3.7. Trim the slices in the beginning and end that do not intersect embryo tissues. For this, select **Image | Stacks | Tools | Slice remover** and specify the first and last slice to remove, making sure to change the “increment” to 1 (otherwise it removes only every other slice).

3.4.3.8. After repositioning and trimming the new dataset make sure to save as a new TIFF file. If this dataset is too large (more than the GPU RAM) consider using BigDataViewer to export as XML/DHF5, as explained in step 3.3 (from the “Image dataset pre-processing” section).

### 3.5. OPT dataset pre-processing and reconstruction

3.5.1. Use the protocol for OPT dataset pre-processing and reconstruction extensively described in Martins et al.<sup>19</sup> and Gualda et al.<sup>28</sup>.

## 4. 3D rendering, visualization and analysis

NOTE: Here we provide a list of possible applications of different software tools, that allow or enhance the visualization and analysis of 3D imaging datasets.

### 4.1. 3D rendering and visualization using Drishti

NOTE: Drishti<sup>40</sup> is a free scientific visualization software designed to explore and present 3D and 4D datasets from micro-CT, confocal/multiphoton and light-sheet microscopy. Here we use this software for 3D rendering and visualization of whole-mount immunofluorescence staining (Step 2; “Sample preparation for 3D imaging” section). There are multiple tutorials online to help users understand how to operate Drishti; search online for “Ajay Limaye Drishti 3D tutorials”. Drishti cannot directly read stacks of TIFF files, so they must be converted first to the native “pvl.nc” format.

4.1.1. Run the “drishtiimport.exe” tool, located in the Drishti installation folder: **Files | Load | Files | choose “Grayscale TIFF image files**, and load a single-channel 3D stack, as saved from Fiji/ImageJ. In the case of a multi-channel composite stack, split the channels in Fiji/ImageJ and save each individually. Voxel type is “ushort”; “File”...“Save as”...“TIF”, reply “y” to all questions. In the **Additional information** window asking for voxel size make sure to add the correct “X Y Z” voxel sizes.

4.1.2. Loading \*.pvl.nc files into Drishti and rendering: In the main window of Drishti, **File | Load | Load 1 ( - 4 ) volumes** depending on the number of channels available (as separate files). After loading, press **F2** for high-quality render. This action requires a powerful GPU card. To handle the rendering parameters, “Transfer function editor”, search on the online

tutorials. Once satisfied with the rendering properties proceed to generating an animated rendering.

4.1.3. Go to **View** and activate the **Keyframe editor**. Handle the embryo and position it in the desired starting position. Use the right-mouse button to “drag” the embryo to the center if necessary, or the mouse scroll to zoom. Hit **set keyframe** in **Keyframe editor**, then choose another position, angle or zoom, drag the time-line marker to a different time point and **Set keyframe** again. Now there are 2 keyframes where the embryo is represented in 2 different positions/angles/zoom, and a number of frames in between. Pressing the **Play** button, Drishti can interpolate the missing conditions and play it as an animation. Go to **File | Save image sequence** to save the animated sequence of all frames. This frame sequence can later be opened in Fiji/ImageJ and saved as AVI (**File | Import | Image sequence ... File | Save As | JPEG compression** with a reasonable frame rate (we suggest 15 - 30).

NOTE: Although Drishti allows the saving of \*.wmv videos, it is advisable to instead save as separate frames and only later create an AVI or MOV video format (this can be done using Fiji/ImageJ).

## 4.2. 3D reconstitutions and manual segmentation of tissues using Amira

NOTE: This commercial software allows, manual or automatically/semi-automatically, 3D segmentation of embryonic tissues in 3D datasets. There is an online “Learning Center” for this software with multiple tutorials available <sup>41</sup>. Below are described the basic steps required to manually segment embryonic tissues from immunofluorescence-stained embryos (step 2; “I -Sample preparation for 3D imaging section”). Manual segmentation is much easier after the embryo is correctly positioned in a standard A-P/D-V axis (see the “Image dataset preprocessing” section, step 4.3).

4.2.1 Load a 3D TIFF dataset. Make sure to specify the correct voxel dimensions, when asked. Create and connect a visualization module (e.g, “Orthoslice” or “Volren”) and inspect the dataset in 3D.

4.2.2 Connect the **Label field** (or **Edit New Label Field** in newer versions of Amira). In this software, results of manual segmentation are stored in “materials”, so create one material for each tissue of interest. Use the “lasso” tool for manual segmentation. There are several tutorials available explaining how to perform this (search online for “Amira Segmentation Editor tutorial”).

4.2.3 When finished with segmentation of all tissues of interest, exit the **Segmentation Editor** by switching back to **Project** mode. Having created a new version of the dataset (the “labels field”, which is now attached to the original dataset module) in which pixels belonging to each material have the same value.

4.2.4 Convert these “materials” into 3D objects by generating 3D surface models from the “Labels” dataset. This can be done by attaching a “Generate Surface” module, adjusting parameters as necessary (activate the “compactify”, “border”, “Adjust coords” and “Unconstrained Smoothing” options). Click **Apply** and a new module \*.surf is generated.

4.2.5 Visualizing the surface objects, extracting and exporting individually as \*.obj files. Attach a **Display | SurfaceView** module to the \*.surf module, and inspect in the main viewer. In the “properties” panel of the “SurfaceView” module, in the “Materials” property select **All + All** and click **remove**, so the viewer’s buffer is emptied. Then in the second pull down of the **Materials** property select only one material and click **Add** to the buffer; only that material should be visible.

4.2.6 In the property **Draw style** click in **more options | create surface** and a new \*.surf module is created and added to the project. Rename it to the name of the tissue (press F2 on the keyboard), and **File | Export Data As...** and **Save as type: Wavefront (\*.obj)**. Repeat the operation for each material.

NOTE: These \*.obj files, each containing one of the tissues segmented in Amira, can be used by other tools (“3Dviewer” plugin from Fiji/ImageJ and SimLab).

### **4.3. Interactive 3D visualization within in a portable document format (PDF) using SimLab Composer**

NOTE: This 3D Computer Graphics software facilitates the creation of surface rendered images, animations and simulations. Useful tutorials can be found on line <sup>42</sup>. Here we describe how this software enables the creation of 3D PDF interactive illustrations, using the wavefront(\*.obj) 3D surface files created with Amira (Step 2.3; “3D rendering, visualization and analysis” section).

4.3.1. Go to **File | New** and create an **empty scene**. Then **File | import** and import the 1st \*.obj file saved from Amira. Keep all options of the **Import file** window unticked and click **OK**.

4.3.2. If nothing appears in the Composer’s display window, click **Ctrl+F** or the icon to **Fit all**. Now the segmented object should appear in the center of the window. Repeat the process to add another segmented object and confirm its position relative to the 1st one (for example, 2 adjacent somites).

4.3.3. Select one of the objects in the display window by clicking with the left mouse button, change its name to reflect the name of the anatomical structure or tissue, then switch to the “3DGeom~1” representation, and using the **Materials** panel, change the color by altering the R,G,B values.

4.3.4. Repeat for all objects, until the 3D illustration is fully assembled. Note that some materials can also be made transparent by manipulating the “Alpha” channel, next to the RGB values, and thereby allow observation of internal or occluded objects.

4.3.5. With this software the assembled embryo illustration can be exported as a “3D PDF” file, which can be included in publications. First create a “template” with text and active links to change “Scene states” to be able to include instructions and three different stages in the same illustration. This can be done by switching from “Scene building” to “Sharing” mode (buttons on the left of the Composer window), then clicking in **Show PDF settings**, and

creating a new page template. To create a simple interactive figure to include in a manuscript, do not use a template and simply **Export PDF**.

NOTE: Use Adobe Acrobat Reader software to interact with the 3D PDFs (operability of the functions in the interactive 3D PDF illustration may vary depending on versions of Acrobat Reader available). Most other viewers are not compatible with the 3D PDF format, including web browsers. Such 3D PDF interactive illustrations can be included in publications; ask editors about this possibility in advance.

#### **4.4. 3D visualization and analysis using Imaris**

NOTE: This software allows comprehensive imaging visualization, analysis and interpretation of 2D-4D microscopy datasets, with intuitive interface and workflows. There are several useful tutorials online on how to get started with this software, available at the website (<https://imaris.oxinst.com/tutorials>). To load and interact more effectively with large datasets in Imaris (typically, those larger than the GPU memory) it is advisable to convert the dataset first to “\*.ims”, using the “ImarisFileConverter.exe” program installed in the Imaris installation folder. The ImarisFileConverter can read many microscopy image formats, including OME and “h5” files as saved by Fiji’s BigDataViewer.

##### **4.4.1. 3D visualization**

4.4.1.1. This software can render a 3D visualization of the dataset using the “3D View” mode and the user is able to make several adjustments to how the dataset is displayed [e.g., choose between MIP (Maximum intensity Projection) or blend mode (better rendering with depth cues and shadows)].

4.4.1.2. “Orthogonal views” mode - With proper embryo positioning (Step 4.3; “Image dataset pre-processing” section) one can use the “Section” tab and navigate through the entire embryo and see optical sections from the normal planes (transverse, coronal and sagittal). If embryos are not properly repositioned, interpreting their anatomy with orthogonal planes is extremely difficult (see **Supplemental Figure 3**). Although Imaris has a function known as “reference frame” to work around this problem when analyzing 3D embryos, it is preferable to reposition the datasets a priori.

##### **4.4.2. 3D analysis**

NOTE: This software also has several tools for analyzing morphology and fluorescence intensities. As an example, here we describe a simple workflow to analyse tissue fluorescence intensity variations over time using the Imaris “Spots” tool, where the user manually places spheres in the embryo in 3D, and Imaris can then measure the tissue fluorescence inside these spheres.

4.4.2.1. Load a 3D or 4D dataset in Imaris and **add new spot** in the **3D view** mode. Then, one can select specific points of the embryo (also during several time points if one uses a 4D dataset) and quantify inside those spots, for example, the intensity mean.

NOTE: This software also allows plotting the intensity over time. This allows the user to easily answer questions like: “how does the fluorescence change inside a somite over time?”.

4.4.2.2. Add the **spot** module by clicking on the **Add new spot** button or selecting **3D view | Spots** in Imaris menu. Choose **Skip automatic reaction, edit manually**. Switch the Imaris pointer mode from **Navigate** to **Select** (this can also be done by hitting the **ESC** key on the keyboard).

4.4.2.3. On the **Spots** properties window, select the **Specific channel** to which the spot will be attached (e.g., “Channel 1”), and activate in **Manual tracking** the **Auto-connect to selected spot** and the **Enable delay before auto-advancing** options.

4.4.2.4. Move the mouse cursor to the visualization window and the cursor should change to a hollow yellow wire sphere. Go to time-point 1 and add a spot (=sphere) by clicking in the tissue of interest. The sphere (“Spot”) is only added if clicking while holding the **shift** key. Repeat for all the desired time points making sure to track the same portion of tissue over time.

4.4.2.5. In the **Spots** properties window, switch to the **Statistics** tab, and inside the **Statistics** switch from **Overall** to **Detailed** statistics. From the first pulldown choose **Specific values**, and from the second pulldown choose “Intensity mean Ch=\*...”, where Ch\* is the channel in which the measurement will be performed. A button right to the “Click to open time-plot panel” will be found in the bottom left of the spots properties window. Clicking this button opens up a plot with the median fluorescence intensity inside the “spots”, plotted over time. These values can also be exported to a spreadsheet for further analysis.

## **REPRESENTATIVE RESULTS:**

The representative results shown in this paper for both the live and the immunofluorescence imaging, were obtained using a two-photon system, with a 20 × 1.0 NA water objective, the excitation laser tuned to 960 nm, and GaAsP photodetectors (as described in Dias et al. (2020)<sup>43</sup>. Optical projection tomography was done using a custom built OPenT scanner (as described in Martins et al. (2009)<sup>19</sup>.

### **Live imaging (4D analysis)**

A representative analysis of LuVeLu reporter activity in mouse embryos during axial extension, obtained according the described protocols for “Sample preparation for live imaging” (Step 1; “Sample preparation for 3D imaging” section), “Live imaging dataset pre-processing” (Step 3; “Image dataset pre-processing” section) and “3D visualization and analysis using Imaris” (Step 4; “3D rendering, visualization and analysis”) can be observed in **Figure 1** and **Video 1**.

### **3D visualization and analysis**

A representative result for the use of immunofluorescence assays to detect potential NMPs and key regulators of mesoderm differentiation, obtained following the protocols described for “Sample preparation for immunofluorescence microscopy” (“Sample preparation for 3D imaging” section, step 2), “Deconvolution” and “Immunofluorescence imaging dataset pre-processing” (“Image dataset preprocessing” section, step 3.2 and 3.4 respectively), and “3D

visualization and analysis using Imaris" ("3D rendering, visualization and analysis", step 4) can be observed in **Figure 2**.

### **3D renderization of immunofluorescence stainings**

**Video 2** shows a representative result for an immunofluorescence assay to detect potential NMPs obtained according to the described protocols for "Sample preparation for immunofluorescence microscopy" (Step 1.2; "Sample preparation for 3D imaging" section), the "Deconvolution" and "Immunofluorescence imaging dataset pre-processing" (Step 3.2 and 3.4, respectively; "Image dataset pre-processing" section), and the "3D rendering and visualization using Drishti" (Step 4.1; "3D rendering, visualization and analysis" section).

### **3D reconstructions**

**Video 3** was generated following the described methods for "Sample preparation for immunofluorescence microscopy" (Step 1.2; "Sample preparation for 3D imaging" section), "Immunofluorescence imaging dataset pre-processing" (Step 3.4; "Image dataset pre-processing" section), and "3D reconstructions and manual segmentation of tissues using Amira" (Step 4.2; "3D rendering, visualization and analysis"). It shows a 3D reconstruction, based on immunofluorescence staining, of the caudal tissues of a E9.5 wild type (WT) mouse embryo.

### **Interactive 3D illustrations**

In **Figure 3** we present an interactive 3D visualization of a reconstruction of the caudal tissues of mouse embryos in a portable document format (3D PDF), prepared following the described protocols for "Sample preparation for immunofluorescence Sample preparation for 3D imaging" section), "Immunofluorescence imaging dataset pre-processing" (Step 3.4; "Image dataset preprocessing" section), "3D reconstructions and manual segmentation of tissues using Amira", and "Interactive 3D visualization within in a portable document format (PDF) using SimLab" ("3D rendering, visualization and analysis", Step 4.2 and 4.3 respectively). This type of format can be easily used to facilitate communicating scientific contents to a more general audience, particularly in a teaching environment. Interactive visualization requires the use of Adobe Acrobat Reader (allow the 3D plugin).

### **OPT dataset visualization**

**Video 4** shows a representative example of an OPT reconstructed dataset, after imaging a E18.5 mouse fetus. Sample was prepared as described in protocols for "Sample preparation for optical projection tomography" ("Sample preparation for 3D imaging" section, step 1.3) the "OPT dataset pre-processing and reconstruction" (step 3.5) and the "3D rendering, visualization and analysis" (step 4). A detailed quantification analysis (e.g., measurements) can also be performed in this dataset using Fiji/ImageJ, Amira or the Imaris software. The movie contains four video segments: the first shows a sequence of black and white sagittal slices produced with Fiji/ImageJ; the second, orthogonal views produced with Imaris showing interactive 3D slicing and rendering of orthogonal tissue portions; the third shows the fetus "assembling" from colored sagittal slices, as prepared in Amira; the last video segment display an animation of the fetus in 3D from different views, prepared with Drishti.

## **FIGURE AND TABLE LEGENDS:**

**Table 1 - Fixation times for embryos at different developmental stages.**

**Table 2 - Generic information to guide the selection of the imaging technique/microscope more suitable for the researcher's specific experimental goal.**

**Video 1 - Two-photon live imaging of *LuVeLu* reporter expression in *Snai1-cKO* and control E8.5 embryos (adapted from ref. 43).** The first segments show the reporter activity at time = 0 (z-stack of 5  $\mu\text{m}$  step-size) and the second parts contains the full live imaging (10  $\mu\text{m}$  z-stacks every 8.5 min).

**Video 2 - 3D renderization of a whole-mount immunofluorescence staining for T (Brachyury) and Sox2 of a E10.5 wild type tailbud.** T expression is shown in magenta, Sox2 in yellow and DAPI in grey.

**Video 3 - 3D reconstruction of a late E9.5 wild type mouse embryo, with a focus on the counteracting of different caudal tissues including mesoderm.**

**Video 4 - E18.5 wild-type embryo as imaged with optical projection tomography, highlighting the in toto imaging and several techniques for visualizing and rendering 3D datasets.** The first segment shows a sequence of sagittal slices prepared in Fiji/ImageJ, the second "live" orthogonal views as rendered in Imaris, the third a sequential rendering from colored sagittal slices prepared in Amira, and the fourth an animated rendering prepared in Drishti.

**Figure 1: 4D analysis of *LuVeLu* reporter expression in E8.5 *Snai1-cKO* and control embryos (adapted from ref. 43).** (A) Snapshot at time-point = 0 of the *LuVeLu* reporter, in *Snai1-cKO* (*Meox2-Cre<sup>+/-</sup>::Snai1<sup>flox/-</sup>*) (Aa) and control (Ab) embryos. In addition to the normal *LuVeLu* signal in the presomitic mesoderm, *Snai1-cKO* embryos also display *LuVeLu* expression in the ectopic bulge that arises from the primitive streak (white arrows). (B) *Snai1-cKO::LuVeLu<sup>+/-</sup>* temporal intensity mean quantitative analysis in the region highlighted by the red spot (Ba) indicates the existence of two-peaks (at  $t = 1.3$  h and  $t = 3.6$  h of the time-lapse) and a substantial decrease between them, therefore suggesting cycling activity in the bulge of the conditional mutant embryo. No signs of *LuVeLu* cycling activity were observed near the primitive streak (green spot; Bb) in *LuVeLu<sup>+/-</sup>* control embryos. Scale bar: 50  $\mu\text{m}$ .

**Figure 2: Whole-mount immunohistochemistry in E9.5 *Snai1-cKO* and WT embryos (adapted from ref. 43).** (A) Immunostainings for T (green) and Sox2 (red). (B) Immunostainings for Tbx6 (green) and Lam1 (red). DAPI is shown in blue. 3D rendering (blend mode) of the caudal part of the different embryos (Aa, Ab, Ba, and Bb). Transversal (Aa1, Ab1, Ba1, Ba2, Bb1 and Bb2) and sagittal (Aa2, Ab2, Ba3 and Bb3) optical sections together with magnifications (Mag.) are also shown for the different embryos. Magnifications are shown without DAPI. White arrows highlight differences in the location of some NMPs (T and Sox2 double-positive cells) in the mutant embryos. Yellow arrows and arrowheads point to ectopic/abnormal Tbx6 and Lam1 expression respectively, in the *Snai1-cKO* embryos. Scale bars correspond to 50  $\mu\text{m}$ .

**Figure 3 - 3D PDF - Interactive 3D illustration in 3D PDF format showing the 3D reconstructions of segmented caudal tissues of wildtype mouse embryos during axial extension (E8.5, E9.5 and E10.5).** Segmentation was done manually in Amira, and the 3D PDF



was assembled and exported in Simlab Composer. Interactive visualization requires Adobe Acrobat Reader (allow the 3D plugin).

**Supplemental Figure 1** - Representative result of a bleached embryo (after Step 3.2; “Sample preparation for 3D imaging” section).

**Supplemental Figure 2** - Representative result of Z-depth signal attenuation (Step 4.1; “Image dataset pre-processing” section). A - before Z-depth signal attenuation; B - good Z-depth signal attenuation; C - incorrect Z-depth signal attenuation.

**Supplemental Figure 3** - Representative result of a whole-mount immunofluorescence staining showing and E7.5 mouse embryo that has been repositioned (A) (following Step 4.3; “Image dataset pre-processing” section) versus the same embryo without being repositioned (B). Visualization was obtained using Imaris (see Step 4.1.2; “3D rendering, visualization and analysis” section). T in yellow, Sox2 in magenta and DAPI in blue.

## DISCUSSIONS:

Axial elongation and segmentation are two of the most complex and dynamic processes occurring during vertebrate embryonic development. The use of 3D and 4D imaging with single-cell tracking has been applied, for some time, to study these processes in both zebrafish and chicken embryos, for which accessibility and culture conditions facilitate complex imaging<sup>19,44-49</sup>. In contrast, the mid and late organogenesis stages of the mouse embryo remain poorly studied in such detail, although some advances have been made, for example in intravital imaging<sup>50</sup>. In this manuscript we provide specific protocols for several methodologies that can be used for the acquisition of multidimensional images and their analysis to facilitate the study of NMPs and their mesoderm derivatives during neck, trunk and tail formation. Although these protocols were designed for mouse embryos, they can be easily tuned to work for explant systems and in vitro models such as 3D embryonic stem cell aggregates like gastruloids<sup>51,52</sup>. Indeed, if applied to human gastruloids<sup>53</sup> these methods would facilitate a better in toto imaging and data analysis of human axial elongation and segmentation, especially given the compatibility of these in vitro model systems with long-term 4D live imaging. In addition to these protocols, we also provide general information about different available microscopy techniques and how they can be used to fit specific experimental goals. We hope this information helps researchers to improve their experimental designs and to take full advantage of the microscopy equipment and image analysis tools available in their laboratories and institutions.

Sample preparation is one of the most important steps of the protocols described in this manuscript, as proper preservation and processing of the embryo during the whole procedure, from dissection to mounting in the microscope, is essential to obtain high quality data. Dehydration (and rehydration), bleaching and clearing procedures are the most critical steps during sample preparation, strongly influencing the final outcome of the imaging. Therefore, we have detailed these steps in our protocol and provided tips that will help researchers to achieve a spotless preparation of their samples. Particularly, we have detailed the use of three different solutions for clearing post-implantation mouse embryos (up to E11.5). Although methyl salicylate and BABB have been used for several years and are efficient clearing reagents, complete laser penetration in some tissues, particularly

mesoderm, is sometimes difficult to achieve. Conversely, RapiClear was found to be very effective in clearing mouse embryos at these developmental stages. In our hands, it proved to enable complete laser penetrance in the various embryonic tissues and, since it is not toxic and does not require embryo dehydration, it greatly simplifies the key step of mounting the embryos in the microscopy slide. Also, to overcome the necessity of manipulating the embryos in the slide (cleared embryos become very fragile and difficult to manipulate once they are transparent) and the use of commercial software (e.g., Amira or Imaris), we have provided a simple but efficient pipeline, using Fiji/ImageJ (free open-source software), that allows embryo repositioning to an anatomically standard/specific position during image pre-processing without losing data quality. Therefore, we expect the methods and details that we provide in this manuscript to facilitate and contribute to improve the key step of sample preparation during immunofluorescence assays.

During image acquisition, it is important to consider the configuration of the system, which affects how samples need to be maintained for live imaging or mounted for optimal observation in 3D. For example, mouse embryos require a heating source, high levels of O<sub>2</sub> and liquid nutrient-rich media (not solid), making it more difficult to be kept live in a microscope with an upright, or a conventional light-sheet configuration. For correct 3D imaging of embryos, immobilization is also important. Available optics is also another important factor to consider; for proper 3D imaging, high numerical aperture objectives should be preferred however those are not always available, especially when large working distances are required (more than a few hundred micrometers). Physiological (i.e., “dipping”) lenses are very common for live imaging however these are not ideal for imaging through a glass-bottom dish or for cleared samples mounted on BABB or methyl salicylate. Although objectives optimized for cleared tissues are becoming more common, they are still relatively rare to find in most laboratories. It is also possible to image cleared tissues with conventional objectives however users must be aware of the limitations and the necessary care before interpreting and analyzing the datasets, as we explain in the sections above. Furthermore, accurate detection and interpretation of imaging results always require careful choice not only of the instrument but also of the operating conditions and setting of parameters. Users are encouraged to read the following reviews<sup>54-57</sup> to fully understand the principles of proper digital imaging and interpretation of bioimages.

Immunofluorescence applied to (2D) histological sections has been the hallmark of studies seeking to understand tissue and cell organization inside embryos. The emergence of whole-mount immunolabeling methods and non-destructive 3D imaging techniques (as those described here) has provided developmental biologists with the means to investigate tissue and cell spatial organization in intact embryos, where it is easier and more accurate to understand gene and protein expression and their relationship to morphogenetic processes. With in toto imaging, it is now possible to perform virtual histology (virtual sectioning in arbitrary slices; **Supplemental Figure 3**), and the 3D visualization and analysis tools can be used to easily explore different hypotheses about cell and tissue architecture and communication (see **Figure 2**, **Video 2** and **Video 4**). Considering that many journals (e.g., eLife and Development) are now giving the opportunity to include videos in the online version of the paper, we urge researchers to take advantage of this opportunity and not only perform 3D and 4D imaging experiments and analysis but also to make 3D videos highlighting their results. This important change in the way data is presented and published, will enable a better

comprehension of the results by the researchers and their peers. Ultimately, these methods have the potential to improve our understanding of vertebrate segmentation, particularly regarding the role of NMPs (Attardi et al. (2018)<sup>45</sup> and Dias et al. (2020)<sup>43</sup> are two good examples).

In this work we have highlighted how the use of some software tools (e.g., Amira and Imaris, but also free open-source tools like Fiji/ImageJ and Drishti) allows and enhances 3D data visualization and analysis in the context of vertebrate axial extension and somitogenesis. In most cases, like for several bioinformatic tools, the software described here can potentially be replaced by another (i.e., there are several software solutions and redundancies). However, we find that the “3D View” function in Imaris allows a 3D visualization with much better quality than the one obtained using the “3D Viewer” Fiji/ImageJ plugin, allowing for example to choose between MIP or blend modes. In addition, we find the “Orthogonal Views” function in Imaris and its pipeline for 3D analysis and quantification (e.g., “Spot” module) user friendlier. In this matter, although practically all software tools allow some form of 3D rendering, we recommend Drishti because of its unique light model and shading which enables the generation of highly realistic renderizations (see last segment of **Video 4**). The rule of thumb for all bioinformatic processing of image datasets (pre-processing and 3D renderings) is that the end result must remain a faithful representation of what is observed in the embryo. Therefore, we provided simple methods to mitigate the problems created by Z-axis scaling distortion (due to refractive index mismatch) and depth signal attenuation (caused by light scattering in deep samples) which severely affect the quality and interpretation of the image datasets. Using these algorithms, we provided instructions to manually segment and 3D reconstruct mesodermal tissues from whole-mount immunofluorescence stainings, by manual contouring (often not possible with tools of automated segmentation) using the Amira software. We find this software especially useful for manual counterstaining of tissues where there is no clear physical separation or contrast differences between them (e.g., expression of a specific transcription factor). A non-commercial recommended alternative for Amira, although less powerful, is the LabKIT Fiji/ImageJ plugin (<https://imagej.net/Labkit>).

We have also included among the representative results an example of a 3D visualization of in toto E18.5 mouse fetus imaged with optical projection tomography, which extends the capabilities of optical imaging and 3D image analysis to the entire mouse embryogenesis<sup>22</sup>. These methodologies can be used to understand and analyze (e.g., through morphological measurements) skeletal abnormalities, like fused vertebrae, scoliosis or spondylocostal dysostosis, that can later occur due to problems during somitogenesis (e.g., *Lfng* mutation)<sup>13, 58-62</sup>. Importantly, this imaging approach allows observation of skeletal malformations in a global context, including other tissues (e.g., muscles) that could also contribute to the phenotypes affecting the vertebral column<sup>63</sup>.

Finally, and in agreement with recent work highlighting volumetric models made with imaging datasets from the eMouse Atlas Project<sup>64</sup>, we have described a detailed step-by-step method that can be used both to illustrate the power of 3D models (e.g., 3D PDF) to a more general audience and to help in the study and teaching of vertebrate axial elongation and segmentation. We hope the information presented in this manuscript contributes to changing

the way researchers design, analyze and present their experiments, and to improve our knowledge of vertebrate body axis formation.

#### ACKNOWLEDGMENTS:

We would like to thank Olivier Pourquié and Alexander Aulehla for the LuVeLu reporter strain, the SunJin laboratory for the RapiClear test sample, Hugo Pereira for the help using BigStitcher, Nuno Granjeiro for helping to set up the live imaging apparatus, the IGC animal facility and past and present members of the Mallo lab for useful comments and support during the course of this work.

We thank the technical support of IGC's Advanced Imaging Facility, which is supported by Portuguese funding ref# PPBI-POCI-01-0145-FEDER-022122 and ref# PTDC/BII-BTI/32375/2017, co-financed by Lisboa Regional Operational Programme (Lisboa 2020), under the Portugal 2020 Partnership Agreement, through the European Regional Development Fund (FEDER) and Fundação para a Ciência e a Tecnologia (FCT, Portugal). Work described in this manuscript was supported by grants LISBOA-01-0145-FEDER-030254 (FCT, Portugal) and SCML-MC-60-2014 (Santa Casa da Misericórdia, Portugal) to M.M., the research infrastructure Congento, project LISBOA-01-0145-FEDER-022170, and the PhD fellowship PD/BD/128426/2017 to A.D.

#### DISCLOSURES:

The authors declare no conflicts of interest.

#### REFERENCES:

1. Wilson, V., Olivera-Martinez, I., Storey, K.G. Stem cells, signals and vertebrate body axis extension. *Development*. **136** (12), 2133–2133 (2009).
2. Dias, A., Aires, R. Axial Stem Cells and the Formation of the Vertebrate Body. *Concepts and Applications of Stem Cell Biology*. 131–158 (2020).
3. Tzouanacou, E., Wegener, A., Wymeersch, F.J., Wilson, V., Nicolas, J.F. Redefining the Progression of Lineage Segregations during Mammalian Embryogenesis by Clonal Analysis. *Developmental Cell*. **17** (3), 365–376 (2009).
4. Aires, R., Dias, A., Mallo, M. Deconstructing the molecular mechanisms shaping the vertebrate body plan. *Current Opinion in Cell Biology*. **55**, 81–86 (2018).
5. Wymeersch, F.J. et al. Position-dependent plasticity of distinct progenitor types in the primitive streak. *eLife*. **5** (JANUARY2016), e10042 (2016).
6. Koch, F. et al. Antagonistic Activities of Sox2 and Brachyury Control the Fate Choice of Neuro-Mesodermal Progenitors. *Developmental Cell*. **42** (5), 514–526 (2017).
7. Chapman, D.L., Papaioannou, V.E. Three neural tubes in mouse embryos with mutations in the T-box gene Tbx6. *Nature*. **391** (1991), 695–697 (1998).
8. de Lemos, L., Dias, A., Nóvoa, A., Mallo, M. EphA1 is a cell surface marker for neuromesodermal progenitors and their early mesoderm derivatives. *bioRxiv*. 584524 (2020).
9. Takada, S., Stark, K.L., Shea, M.J., Vassileva, G., McMahon, J.A., McMahon, A.P. Wnt-3a regulates somite and tailbud formation in the mouse embryo. *Genes and Development*. **8** (2), 174–189 (1994).
10. Chalamalasetty, R.B. et al. Mesogenin 1 is a master regulator of paraxial presomitic mesoderm differentiation. *Development*. **141** (22), 4285–4297 (2014).
11. Pais-de-Azevedo, T., Magno, R., Duarte, I., Palmeirim, I. Recent advances in

- understanding the mechanisms determining longevity. *F1000Research*. **7**, 97 (2018).
12. Hubaud, A., Pourquié, O. Signalling dynamics in vertebrate segmentation. *Nature Reviews Molecular Cell Biology*. **15** (11), 709–721 (2014).
13. Pourquié, O. Vertebrate segmentation: From cyclic gene networks to scoliosis. *Cell*. **145** (5), 650–663 (2011).
14. Mallo, M. Revisiting the involvement of signaling gradients in somitogenesis. *FEBS Journal*. **283** (8), 1430–1437 (2016).
15. Boulet, A.M., Capecchi, M.R. Signaling by FGF4 and FGF8 is required for axial elongation of the mouse embryo. *Developmental Biology*. **371** (2), 235–245 (2012).
16. Dickinson, M.E. et al. High-throughput discovery of novel developmental phenotypes. *Nature*. **537** (7621), 508–514 (2016).
17. McDole, K. et al. In toto Imaging and Reconstruction of Post-Implantation Mouse Development at the Single-Cell Level. *Cell*. **175**, 859–876 (2018).
18. McColl, J., Mok, G.F., Lippert, A.H., Ponjavic, A., Muresan, L., Münsterberg, A. 4D imaging reveals stage dependent random and directed cell motion during somite morphogenesis. *Scientific Reports*. **8** (1), 12644 (2018).
19. Martins, G.G., Rifes, P., Amaândio, R., Rodrigues, G., Palmeirim, I., Thorsteinsdóttir, S. Dynamic 3D cell rearrangements guided by a fibronectin matrix underlie somitogenesis. *PLoS ONE*. **4** (10), e7429 (2009).
20. Bénazéraf, B. et al. Multi-scale quantification of tissue behavior during amniote embryo axis elongation. *Development*. **144** (23), 4462–4472 (2017).
21. Sharpe, J. Opticam Projection Tomography. *Advanced Imaging in Biology and Medicine*. 199–224 (2009).
22. Sharpe, J. et al. Optical projection tomography as a tool for 3D microscopy and gene expression studies. *Science*. **296** (5567), 541–545 (2002).
23. Aulehla, A. et al. A beta-catenin gradient links the clock and wavefront systems in mouse embryo segmentation. *Nature Cell Biology*. **10** (2), 186–193 (2008).
24. Osorno, R. et al. The developmental dismantling of pluripotency is reversed by ectopic Oct4 expression. *Development*. **139** (13), 2288–2298 (2012).
25. Bryson-Richardson, R.J., Currie, P.D. Optical projection tomography for spatio-temporal analysis in zebrafish. *Methods in Cell Biology*. **76**, 37–50 (2004).
26. Quintana, L., Sharpe, J. Optical projection tomography of vertebrate embryo development. *Cold Spring Harbor Protocols*. **6** (6), 586–594 (2011).
27. Cho, A., Suzuki, S., Hatakeyama, J., Haruyama, N., Kulkarni, A.B. A Method for Rapid Demineralization of Teeth and Bones. *The Open Dentistry Journal*. **4** (1), 223–229 (2010).
28. Gualda, E.J., Vale, T., Almada, P., Feijó, J.A., Martins, G.G., Moreno, N. OpenSpinMicroscopy: An open-source integrated microscopy platform. *Nature Methods*. **10** (7), 599–600 (2013).
29. Schindelin, J. et al. Fiji: An open-source platform for biological-image analysis. *Nature Methods*. **9** (7), 676–682 (2012).
30. Weigert, M. et al. Content-aware image restoration: pushing the limits of fluorescence microscopy. *Nature Methods*. **15** (12), 1090–1097 (2018).
31. Krull, A., Buchholz, T.O., Jug, F. Noise2void-learning denoising from single noisy images. *2019 IEEE. In CVF Conference on Computer Vision and Pattern Recognition (CVPR)*. 2124–2132 (2018).
32. Sage, D. et al. DeconvolutionLab2: An open-source software for deconvolution microscopy. *Methods*. **115**, 28–41 (2017).

33. Pietzsch, T., Saalfeld, S., Preibisch, S., Tomancak, P. BigDataViewer: Visualization and processing for large image data sets. *Nature Methods*. **12** (6), 481–483 (2015).
34. Parslow, A., Cardona, A., Bryson-Richardson, R.J. Sample Drift Correction Following 4D Confocal Time-lapse Imaging. *Journal of Visualized Experiments*. **86**, e51086 (2014).
35. Hörl, D. et al. BigStitcher: reconstructing high-resolution image datasets of cleared and expanded samples. *Nature Methods*. **16** (September), 870–874 (2019).
36. Ohser, J. et al. Attenuation correction for confocal laser scanning microscopy and its application in chromatography. *Journal of Microscopy*. **278**, 76–88 (2020).
37. Hell, S., Reiner, G., Cremer, C., Stelzer, E.H.K. Aberrations in confocal fluorescence microscopy induced by mismatches in refractive index. *Journal of Microscopy*. **169**, 391–405 (1993).
38. Kuypers, L.C., Decraemer, W.F., Dirckx, J.J.J., Timmermans, J. A procedure to determine the correct thickness of an object with confocal microscopy in case of refractive index mismatch. *Journal of Microscopy*. **218**, 68–78 (2005).
39. Meijering, E.H.W., Niessen, W.J., Viergever, M.A. Quantitative evaluation of convolution-based methods for medical image interpolation. *Medical Image Analysis*. **5** (2), 111–126 (2001).
40. Limaye, A. Drishti: a volume exploration and presentation tool. *Developments in X-Ray Tomography VIII*. 85060X (2012).
41. (<https://www.thermofisher.com/pt/en/home/industrial/electron-microscopy/electron-microscopy-instruments-workflow-solutions/3d-visualization-analysis-software/3d-visualization-analysis-software-resource-center.html>).
42. (<https://www.simlab-soft.com/3d-products/Tutorials/simlab-composer-all-Tutorials.aspx?t=3>).
43. Dias, A. et al. A TgfbRI/Snai1-dependent developmental module at the core of vertebrate axial elongation. *eLife*. **9**, e56615 (2020).
44. Delaune, E.A., François, P., Shih, N.P., Amacher, S.L. Single-Cell-Resolution Imaging of the Impact of Notch Signaling and Mitosis on Segmentation Clock Dynamics. *Developmental Cell*. **23** (5), 995–1005 (2012).
45. Attardi, A. et al. Neuromesodermal progenitors are a conserved source of spinal cord with divergent growth dynamics. *Development*. **145** (21), dev166728 (2018).
46. Romanos, M. et al. Cell-to-cell heterogeneity in Sox2 and Brachyury expression guides progenitor destiny by controlling their movements. *bioRxiv*. 388611 (2020).
47. Guillot, C., Michaut, A., Rabe, B., Pourquié, O. Dynamics of primitive streak regression controls the fate of neuro-mesodermal progenitors in the chicken embryo. *bioRxiv*. 077586 (2020).
48. Steventon, B., Duarte, F., Lagadec, R., Mazan, S., Nicolas, J.F., Hirsinger, E. Species-specific contribution of volumetric growth and tissue convergence to posterior body elongation in vertebrates. *Development*. **143** (10), 1732–1741 (2016).
49. Lawton, A.K. et al. Regulated tissue fluidity steers zebrafish body elongation. *Development*. **140** (3), 573–582 (2013).
50. Huang, Q. et al. Intravital imaging of mouse embryos. *Science*. **368** (6487), 181–186 (2020).
51. Van Den Brink, S.C. et al. Symmetry breaking, germ layer specification and axial organisation in aggregates of mouse embryonic stem cells. *Development*. **141** (22), 4231–4242 (2014).
52. Baillie-Johnson, P., van den Brink, S.C., Balayo, T., Turner, D.A., Martinez Arias, A.

- Generation of aggregates of mouse embryonic stem cells that show symmetry breaking, polarization and emergent collective behaviour in vitro. *Journal of Visualized Experiments*. **2015** (105), e53252 (2015).
53. Moris, N. et al. An in vitro model of early anteroposterior organization during human development. *Nature*. **582** (December 2018), 410–415 (2020).
54. Rossner, M., Yamada, K.M. What's in a picture? The temptation of image manipulation. *The Journal of Cell Biology*. **166** (1), 11–15 (2004).
55. North, A.J. Seeing is believing? A beginners' guide to practical pitfalls in image acquisition. *Journal of Cell Biology*. **172** (1), 9–18 (2006).
56. Jost, A.P.-T., Waters, J.C. Designing a rigorous microscopy experiment: Validating methods and avoiding bias. *Journal of Cell Biology*. **218** (5), 1452–1466 (2019).
57. Jonkman, J., Brown, C.M., Wright, G.D., Anderson, K.I., North, A.J. Tutorial: guidance for quantitative confocal microscopy. *Nature Protocols*. **15** (5), 1585–1611 (2020).
58. Stauber, M., Sachidanandan, C., Morgenstern, C., Ish-Horowicz, D. Differential axial requirements for Lunatic fringe and Hes7 transcription during mouse somitogenesis. *PLoS ONE*. **4** (11), e7996 (2009).
59. Turnpenny, P.D. et al. Abnormal vertebral segmentation and the notch signaling pathway in man. *Developmental Dynamics*. **236** (6), 1456–1474 (2007).
60. Andrade, R.P., Palmeirim, I., Bajanca, F. Molecular clocks underlying vertebrate embryo segmentation: A 10-year-old hairy-go-round. *Birth Defects Research (Part C)*. **81** (2), 65–83 (2007).
61. Sparrow, D.B. et al. Mutation of the LUNATIC FRINGE gene in humans causes spondylocostal dysostosis with a severe vertebral phenotype. *American Journal of Human Genetics*. **78** (1), 28–37 (2006).
62. Giampietro, P.F. et al. Progress in the understanding of the genetic etiology of vertebral segmentation disorders in humans. *Annals of the New York Academy of Sciences*. **1151**, 38–67 (2009).
63. Blecher, R. et al. The Proprioceptive System Masterminds Spinal Alignment: Insight into the Mechanism of Scoliosis. *Developmental Cell*. **42** (4), 388–399 (2017).
64. Vianello, S. Exploring and illustrating the mouse embryo : virtual objects to think and create with. *bioRxiv*. 393991 (2020).

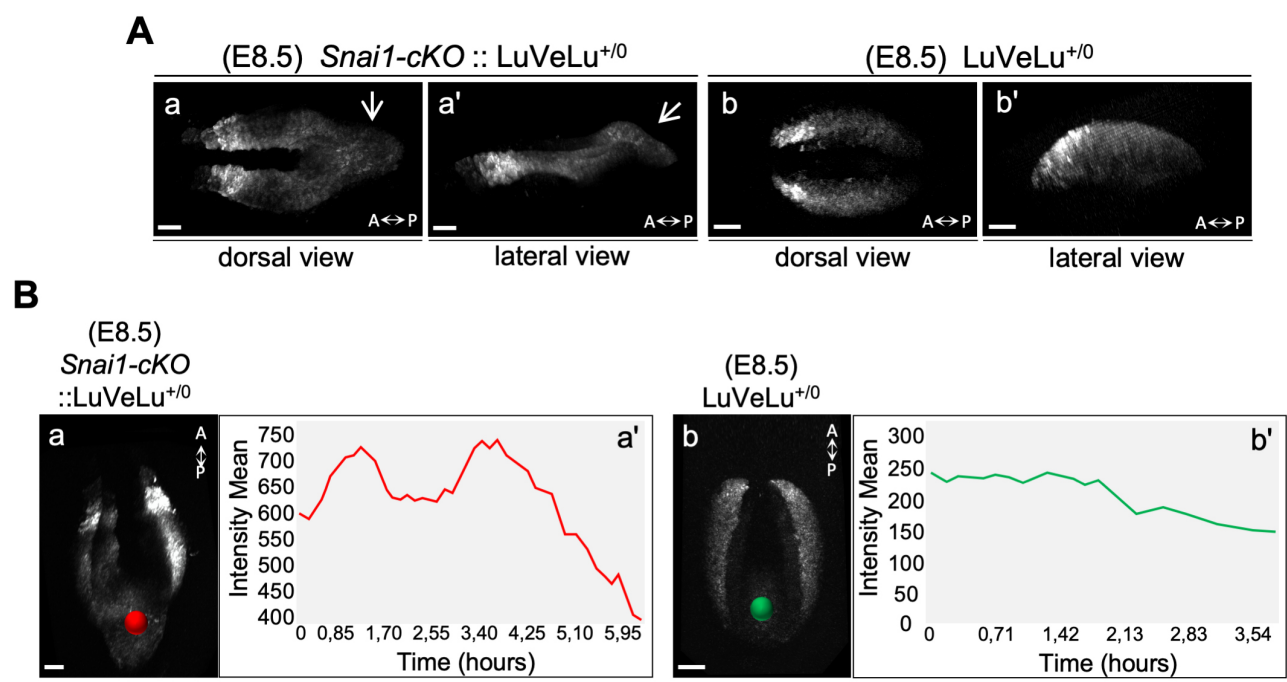


Figure 1



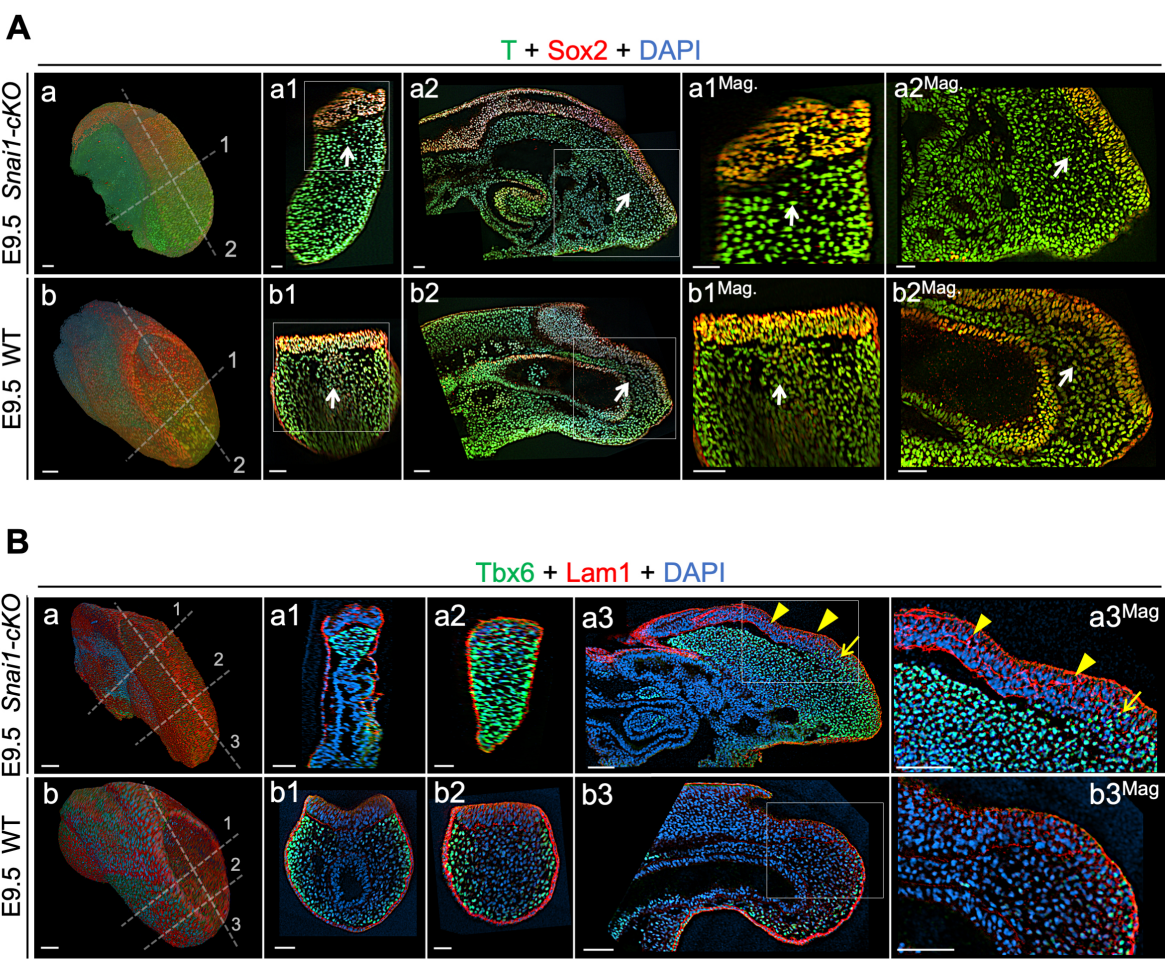


Figure 2

# 3D visualization approaches to study vertebrate segmentation

( SIDE VIEW )

A  
N  
T  
E  
R  
I  
O  
R

P  
O  
S  
T  
E  
R  
I  
O  
R



3D PDF illustration of caudal tissues in WT embryos, stages E8.5 to E10.5

Choose the stage in the bottom row, then click and drag on 3D model to interact

Left mouse click rotates, right zooms. Ctrl+click allows panning.

“Model Tree” function of reader can be used to turn on/off specific tissues.

“Render mode” in toolbar can be switched between “solid” and “transparent”.

\* Must use Adobe Acrobat reader to be able to interact.

Caudal epiblast - light green

Neural tube - green

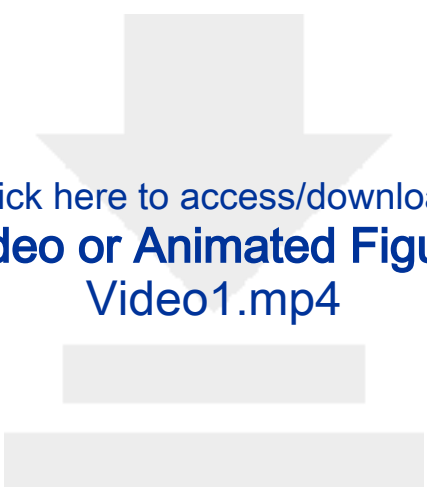
Meosoderm - light blue

Somites - (dark) blue

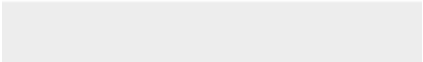

Notochord - red

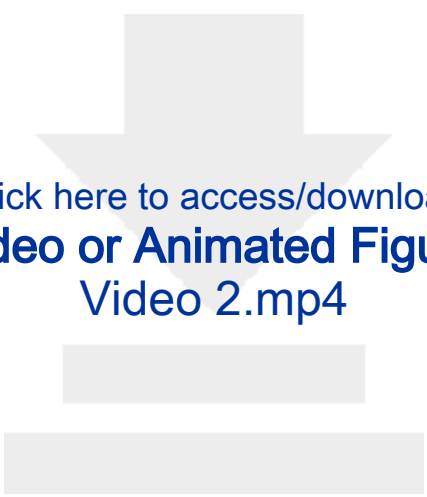
Gut - yellow

scale bar = 100um

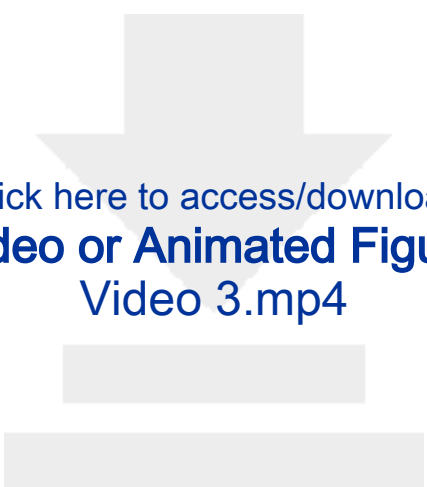


Click here to access/download  
**Video or Animated Figure**  
Video1.mp4

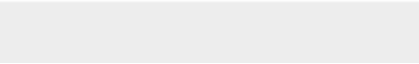



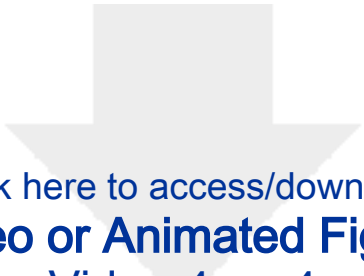


Click here to access/download  
**Video or Animated Figure**  
Video 2.mp4

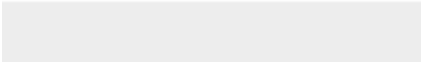



Click here to access/download  
**Video or Animated Figure**  
Video 3.mp4





Click here to access/download  
**Video or Animated Figure**  
Video 4.mp4



Developmental stage	Recommended fixation time (PFA 4%)
E7.5	1h30
E8.5	2h
E9.5	3h
E10.5	4h
E11.5	4h

Optical microscopy techniques

Widefield imaging

Confocal (laser scanning; CLSM)

Two-photon excitation fluorescence  
(TPEFM)

Confocal (spinning disk)

Light-sheet / single plane (LSFM/SPIM)

Optical projection tomography (OPT)

Optical Coherence Tomography (OCT)

Super-resolution (SN), atomic force (AFM)  
or near-field imaging (NSOM)



## Imaging principle

Uses fluorescence, reflected or transmitted light.

Uses laser scanning illumination and detection of fluorescence through a pinhole.

It uses pulsed near-infrared (NIR) laser excitation instead of visible laser illumination.

A form of confocal which, instead of a single laser, uses multiple point-like sources.

Instead of widefield or point-like illumination, the sample is illuminated in one orthogonal plane at a time. In most configurations, it allows imaging from multiple angles.

Optical slices are not detected but calculated from a series of widefield images of the whole embryo from different angles (the “projections”).

Uses NIR illumination through the sample to obtain optical slices based on interference with light reflection.

SR is normally based on single-molecule localization and AFM/NSOM on scanning surfaces at sub-diffraction resolutions (few nanometers).

### Experimental goal and considerations

Ideal for a quick and general overview of the embryo (e.g. for screenings and to assess developmental stages and obvious phenotypes). The reduced depth-of-field, compared to the observable thickness at high magnifications does not allow accurate interpretation or analysis of 3D morphology.

Allows imaging of optical slices of fluorescently-labelled samples, ideally with a strong signal. Imaging through a pinhole removes the signal from out of the depth-of-field, thereby allowing accurate discrimination of information in 3D. The acquisition is orders of magnitude slower than widefield, but with unparalleled contrast and 3D discrimination of morphology. High temporal resolution is not achievable because images are acquired 1-pixel at a time. Good for 3D imaging of fixed mouse embryos up to E9.5. Imaging through the whole presomitic mesoderm or somites requires tissue-clearing, because of light-scattering in deeper tissues. Phototoxicity and bleaching is a consideration. Photobleaching can, within limits, be compensated a posteriori. However, phototoxic effects in live samples cannot, and often are not easy to determine. This is more obvious if samples show low expression, and high-laser powers are needed.

Although more expensive, slightly slower and difficult to operate than the CLSM, the TPEFM allows optical slicing through thicker samples. Resolution is also slightly lower than that obtained with CLSM, but the contrast in deeper tissues is considerably better. Good for live imaging of mouse embryos. TPEFM is often considered less phototoxic than the conventional confocal but requires high laser powers which may also have deleterious effects on cells and tissues. Ideal for 3D imaging of embryos up to E11.5; imaging through the whole presomitic mesoderm still requires tissue-clearing, though.

The use of multiple point-like structures allows faster creation of optical slices (several frames per second or stacks per minute are achievable) than CLSM. The acquisition is practically as fast as widefield, with reasonable 3D discrimination. However, it only allows imaging of the most superficial tissues of the mouse embryo. Allows more sensitive detection than CLSM, making it an alternative for embryos with low expression of fluorescence proteins. Also requires fluorescently-labelled samples. Optical slices acquisition is extremely fast (multiple frames per second) and has reduced effects of phototoxicity or bleaching. However, if multiview is required, subsequent dataset pre-processing steps may require hours/days of computation. LSFM/SPIM allows better detection of lower expression levels than CLSM. Ideal for 3D imaging of *in toto* mouse embryos during gastrulation. Samples need to be mounted and maintained in suspension (unconventional preparation).

Ideal for 3D imaging of later stage mouse embryos/fetuses (>5mm), but only fixed and cleared. Has the advantage of producing 3D stacks of optical slices of both fluorescent and non-fluorescent samples. Datasets are isometric (hundreds of slices with equal resolution in all three dimensions) making it ideal for morphological analysis. Acquiring a projection dataset may require only a few minutes, followed by 15-30 min of reconstruction. It is possible to send samples for imaging remotely.

OCT allows easy imaging through live tissue (a few millimeters deep into the sample without fluorescent contrast) with possibly a few dozen micrometers resolution. The acquisition is very fast (a few slices per second). Although it is a possible alternative for OPT, this technique is not commonly available.

Allows imaging at sub-diffraction level (<200nm resolution), often with the intent to detect single molecules or molecules at the cell surface. Not ideal for morphological analysis of large samples such as mouse embryos. The acquisition is typically a slow process (seconds to minutes per image).

Name of Material/ Equipment	Company
Agarose low gelling temperature	Sigma
Amira software	Thermofisher
Anti-Brachyury (Goat polyclonal)	R and D Systems
Anti-Sox2 (Rabbit monoclonal)	Abcam
Anti-Tbx6 (Goat polyclonal)	R and D Systems
Anti-Laminin111 (Rabbit polyclonal)	Sigma
Anti-goat 488 (Donkey polyclonal)	Molecular Probes
Anti-rabbit 568 (Donkey polyclonal)	ThermoFisher Scientific
Benzyl Alcohol (99+%)	(any)
Benzyl Benzoate (99+%)	(any)
Bovine serum albumin	Biowest
Coverglass 20x20 mm #0	(any)
Coverglass 20x20 mm #1	(any)
Coverglass 20x60 mm #1.5	(any)
DAPI (4',6-Diamidino-2- Phenylindole Dihydrochloride)	Life Technologies
Drishti software	(open source)
EDTA	Sigma
Fiji/ImageJ software	(open source)
Glycine	NZYtech
Huygens software	Scientific Volume Imaging
HyClone defined fetal bovine serum	GE Healthcare
Hydrogen peroxide solution 30 %	Milipore
Imaris software	Bitplane / Oxford instruments
iSpacers	SunJin Lab
L-glutamine	Gibco
Low glucose DMEM	Gibco
M2 medium	Sigma
Methanol	VWR
Methyl salicylate	Sigma
Paraformaldehyde	Sigma
Penicillin-streptomycin	Sigma
PBS (Phosphate-buffered saline solution)	Biowest
RapiClear	SunJin Laboratory
Secure-Sea hybridization chambers	Sigma
simLab software	SimLab soft
Slide, depression concave glass - 75x25 mm	(any)
Triton X-100	Sigma

Catalog Number	Comments/Description
A9414	Used to mounting embryos (e.g. for OPT)
-	Commercial software tool
AF2085 RRID:AB_2200235	For immunofluorescence
ab92494 RRID:AB_10585428	For immunofluorescence
AF4744 RRID:AB_2200834	For immunofluorescence
L9393 RRID:AB_477163	For immunofluorescence
A11055 RRID:AB_2534102	For immunofluorescence
A10042 RRID:AB_2534017	For immunofluorescence
-	Used to clear embryos (component of BABB)
-	Used to clear embryos (component of BABB)
P6154	For immunofluorescence
-	100um thick
-	170um thick
-	To use as “slides”
D3571	For immunofluorescence
-	Free software tool
ED2SS	For demineralization
-	Free software tool
MB01401	For immunofluorescence
-	Commercial software tool
#HYCLSH30070.03	For live imaging
1085971000	For clearing
-	Commercial software tool
(varies)	Use as spacers for preparations
#25030–024	For live imaging medium
11054020	For live imaging medium
M7167	To dissect embryos
VWRC20847.307	For dehydration and rehydration steps
M6752	Used to clear embryos
P6148	Used in solution to fix embryos
#P0781	For live imaging medium
L0615-500	-
RapiClear 1.52	Used to clear embryos
C5474	Use as spacers for preparations
-	Commercial software tool
-	To mount thick embryos.
T8787	For immunofluorescence

Dear Editor,

In the version of the manuscript that we are now submitting we have introduced all the revisions requested in your e-mail from December 22. We have introduced answers to the different questions directly in the manuscript, prepared on the template attached to your e-mail. In addition, as requested, we introduced new figures to replace the reference to figures in our eLife article [Dias et al., (2020) eLife 9,e56615]. After contacting the Journal, we were informed that we could use those figures freely, as we are the owners of the copyright.

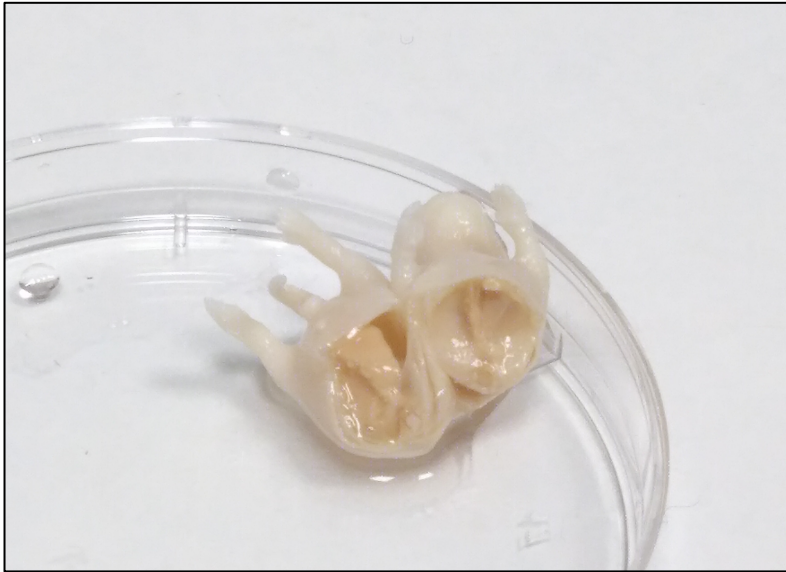
**Figure S1**

Figure S2

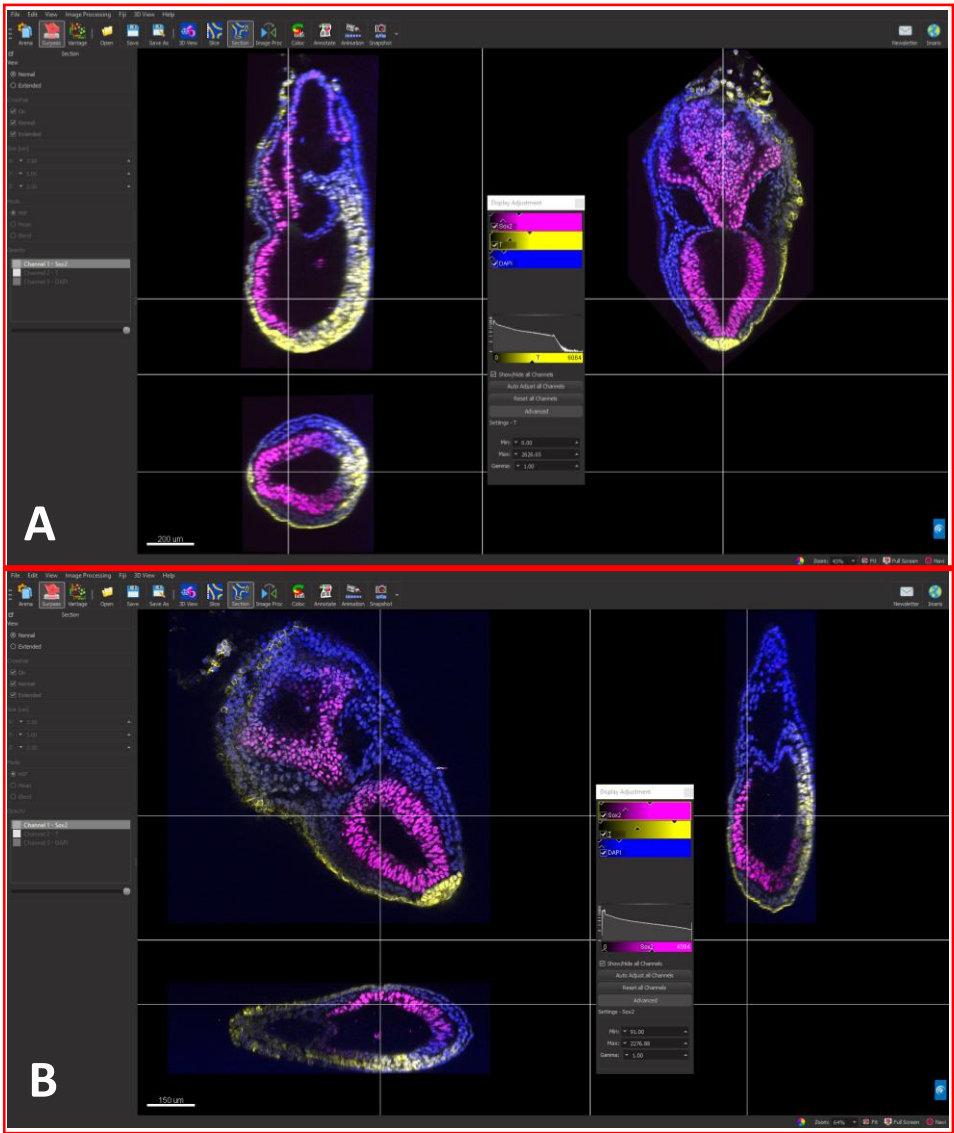


Figure S3

